PCCP

Accepted Manuscript

This article can be cited before page numbers have been issued, to do this please use: H. G. Ozcelik and M. Barisik, *Phys. Chem. Chem. Phys.*, 2019, DOI: 10.1039/C9CP00706G.

ROYAL SOCIETY OF CHEMISTRY

rsc.li/pccp

View Article Online
DOI: 10.1039/C9CP00706G

Electric Charge of Nano Patterned Silica Surfaces

H. Gokberk Ozcelik[1], Murat Barisik[1*]

[1]Department of Mechanical Engineering, Izmir Institute of Technology, IZMIR, 35430

* Corresponding author E-mail: muratbarisik@iyte.edu.tr

Abstract

The most recent technologies employ nanoscale surface patterning or roughening in order to engineer desired properties on a surface. Electrokinetic properties at the interface of such surfaces and ionic liquids show different behavior than the well-known theoretical descriptions. Basically, ionic distribution on the surface differs due to electrical double layer overlap effects in the pits and curvature effects at the tips of surface structures. Generally, the charge density of a surface is assumed to be a material property and surface roughness effects are overlooked in most literature. In contrast, we properly calculated the local surface charges based on surface chemistry at the corresponding local ionic concentration (Charge Regulation) for various surface roughness and solution conditions. Results showed that the surface charge density of silica decreased at the pits but increased at the tips of surface patterns. Even for the simplest case of self-repeating surface structures, the average of local surface charges becomes lower than the theoretical predictions. Based on numerical calculations, a phenomenological model was developed as an extension to the existing flat surface theory, which can successfully predict the average surface charge on a nano patterned surface as a function of surface pattern size, ionic concentration and pH.

Keywords: Surface charge density, charge regulated surface, nanoscale surface patterns, surface roughness.

View Article Online
DOI: 10.1039/C9CP00706G

Electrostatic properties of surfaces play a key role in several recent nano-technologies. When a solid surface meets an aqueous medium, molecular surface groups interact with ionic fluid and form a chemical equilibrium defining the charge property of the solid surfaces. This surface charge determines interactions and transports in nano systems, including particle transport in nanofluidic devices[1], separation processes such as desalination[2,3] , measurement of surface topography[4,5], drug delivery[6,7], DNA and protein transport[8,9], and biological/chemical agent detection[10,11]. The design and performance of these applications requires an accurate knowledge of surface charging mechanisms at various conditions, which is not yet well understood.

Surface charge originates from reactions occurring at interfaces between immersed body and electrolyte solution. [12] The association/disassociation of polar groups and the adsorption of ions creates the surface charge based on the solution properties such as, electrolyte concentration, pH and variety in ions. The charged interface attracts counter ions and forms electric double layer (EDL).[13] In such a context, surface charge and EDL are interrelated; one forms the other. In general, ionic distribution on the surface is described by Boltzmann distribution (BD) by assuming a flat surface sufficiently away from any other bodies. After further simplifications, the electric charge of the corresponding surface is calculated analytically. Many existing studies and applications use such an approach and assume a constant charge density on a surface calculated for the corresponding material. However, the flat surface assumption is very much against the nature showing a variety of surface topologies where ionic distribution on the surface and the resulting electric charge will be different from the BD based descriptions. Assuming the surface roughness or patterns in the form of hills and valleys at nano-scales, divergence from the BD develops in two folds for a non-planar surface. First, for valley spacings comparable with or smaller than the thickness of EDL, ionic layers (EDLs) extending from opposite surfaces overlap, causing the local ionic concentrations differs from the BD. Second, for hill sizes comparable with or smaller than the thickness of EDL, curvature effects develop due to the decreased surface to volume ratio, creating ionic distribution different than the BD again. Curvature effect has been observed by multiple researchers in the surface charge behavior of nano-particles[14,15] . These two occurrences yield local variation of surface charge as a function of surface nano topology which was observed by few studies through AFM measurements[16] and numerical simulations[17,18], but there has not been any proper characterization of the behavior, yet.

View Article Online
DOI: 10.1039/C9CP00706G

Non-homogenous distribution of the charge of a surface can be used to create many interesting mechanisms. The modification of surface charge distribution or surface charge patterning at nano-scale is exercised in a wide range of applications, such as creating anti-bacterial surfaces[19,20], controlling thermodynamic phase behavior of colloids[21,22], designing behavior of nanoparticles[23,24], controlling fluid flow and mixing in Lab-on-a-chips[25,26], developing desired Janus particles[27], controlling cell microenvironments[28,29], or even mimicking organ behaviors in Organ-on-a-chips[30]. However, nano-patterned surface charges are frequently developed using very sophisticated and complicated techniques such as positioning charge or nano patterns using AFM[31] and optical tweezers[32], or controlling self-assembly of biological/chemical groups[33] and nanoparticles[34]. Instead, the manipulation of a local surface charge can be obtained by simply changing the surface topography. The alteration of surface topography or surface patterning is originally employed to modify interfacial energy for the control of wetting, heat transfer and fluid transport. For example, the wetting of a surface can be changed depending on the size and geometry of the structures formed on the surface; hydrophobic behavior can be created for self-cleaning or anti-icing surfaces[35] while a hydrophilic surface can be obtained for more efficient biomedical or heat transfer applications[36]. Since surface patterning is employed by larger communities, fabrication techniques are more established. Nanolithography can be used to construct desired structures or chemical etching can be used to develop fractal structures or femtosecond lasers can be used to ablate surface patterns. The latter approach, becoming popular just recently, is very promising due to its flexibility, simplicity, and controllability in creating several types of nano/microstructures required for a wide range of applications. Manipulation of surface charge by changing surface topography was utilized recently by creating fractal structures as an electrode for enhanced electrophoresis properties[37] and efficiency in detecting biomolecules[38]. But, there is not a proper correlation between surface topography and surface charge. Although surface patterning is a well-known approach to tune surface properties of materials in wide range of application, there is a gap to link local surface charge properties to surface patterning because physical heterogeneity is not the only complication, physical heterogeneity originated local complications such as overlapping of EDLs, curvature, and size effects of asperities should also be considered.

It is also important to mention that one of the most common nanotechnology application determines the topology of a surface under an ionic fluid by measuring the electrostatic pressure

View Article Online
DOI: 10.1039/C9CP00706G

forces on the surface developed from surface charges. The well-known Atomic Force Microscope (AFM) post-processes measured force vs distance curves over a certain point of a substrate to determine the surface location generally using the classical DLVO theory (developed by Derjaguin&Landau[39] and Verwey&Overbeek[40,41]). DLVO describes the interaction force between charged surfaces in a liquid medium by formulizing the two main components of interparticle interaction, van der Waals and EDL forces, based on BD assuming a planar surface. Presence of surface structural variations lead to secondary interactions which can be included by the updated DLVO calculations[42–44] . However, these extensions consider roughness effects as a physical heterogeneity and continued to employ the homogenous surface charge assumption. On the contrary, the presence of roughness trigger further complications on the surface chemistry due to the local ionic variation originated from the EDL overlap in the pits and the curvature effects at the tips of surface structure. Most of the existing AFM calculations disregard this surface charge heterogeneity which can be attributed to the lack of a simple approach to character variation in surface charge by surface topography. Only recently, a few AFM studies underlined this discrepancy and questioned the determination of location of surface based on constant[45,46] and homogenous[16] surface charge assumption; instead, they recommended extending the DLVO theory to consider so-called "Charge Regulation (CR)" nature of surface chemistry[47]. CR was first identified by Ninham and Parsegian[48] and later observed by multiple studies in surface force measurements by colloids [49,50] and AFM [4,51,52]. These studies were conducted on perfectly planar surfaces with known surface location that force measurements were used to determine surface charge, contrary to classical approach of known surface charge and unknown surface location. Through these studies, the CR was mostly deliberated for the variation of the surface charge at a specific surface location due the EDL overlap between the AFM tip and the surface at various separation distances during an AFM force measurement. There are only limited studies considering the surface charge heterogeneity, but even these do no properly characterize or offer an explicit solution for the surface charge behavior of non-planar surfaces.

Other than AFM literature, the calculations of surface charge density as a function of the local ionic environment has been practiced for nanoscale confinements. The numerical solution of ionic distributions is coupled with the CR models as a surface boundary condition. The CR models calculate the effects of the protonation/deprotonation in surface reactions based on the site density of the functional groups. Most of the existing literature focuses on the surface charging

View Article Online
DOI: 10.1039/C9CP00706G

characteristics of straight channels[53–55] and tubes[56,57] where EDL overlap and entrance/exit effects create local variation of surface charge on planar surfaces. There are only a few studies in literature that refer to surface topology effects on surface charging[16–18], but these studies presented their results without examining or describing its occurrence. Hence, there has not been a proper characterization or explicit solution for the surface charge behavior of non-planar surfaces, yet.

The aim of this work is to investigate surface charge density of nano-patterned silica surfaces as a function of pattern size at various solution conditions. Silica is chosen due to its widespread application uses in colloidal science, drug delivery and nanofluidic studies. Previously proposed analytical methods for surface charge calculations are restricted due to employed Debye-Hückel approximation which is applicable only for low surface charge values. Instead, finite element based multiphysics simulations are employed with a multi-ion charge-regulation model[15,58] to solve Poisson-Nernst-Planck equation to consider the effects of EDL overlap and curvature on a patterned surface for the first time in literature.

Theoretical Background and Mathematical Model

In general, ionic distribution on a surface with a given surface charge density obeys the Boltzmann distribution (BD)[59,60] and the potential distribution through a semi-infinite EDL can be calculated by the well-known Poisson-Boltzmann (PB) equation. The Debye-Hückel simplification[61] yields analytical solution of PB equation for low wall potentials (<25mV). The high wall potential cases require solution of complex elliptic functions[62,63] or use of trial error methods to calculate the electric potential.[64,65] However, all these methods are only valid for semi-infinitely extending EDL fields. In the case of EDL overlap where the EDLs growing from opposite surfaces start interacting, using Boltzmann distribution in Poisson equation becomes incorrect.[53,64] The potential distribution with EDL overlap significantly deviates from no-overlap cases obeying the Boltzmann distribution. For such a case, the original form of the Poisson-Nernst-Planck (PNP) theory should be employed in the analyses, in contrast to frequently used simplified versions of PNP.[59,66] Defining surface boundary condition in case of EDL overlap also requires additional attention. In most of the literature, assigning either constant surface charge[67,68] or constant wall potential[69] boundary condition onto the surfaces is the general way to solve PNP. The wall potential (ψ) and surface charge density on the wall (σ_w) are related to each other as given in Equation 1. If constant surface charge density is assumed on overlapping surfaces, the electric potential value at the surface will change by EDL overlap. On the other hand, if a constant wall

View Article Online
DOI: 10.1039/C9CP00706G

potential condition is implied, EDL overlap will cause the change of the surface charge density (*i.e.* slope of the potential distribution at the wall). These cases are common practices in existing literature, [44] however, both approaches do not properly reproduce the nature of surface.

$$-\varepsilon_0\varepsilon_r \underline{\underline{n}}.\nabla\psi = \sigma_w \tag{1}$$

Enforcing constant surface charge or potential at the interface does not represent physical response of the surface chemistry. Surface reactions develop based on the local ionic environment at the interface, that neither surface charge nor potential remain constant; instead, both of them undergo variation in response to the variation in ionic distribution and create a new equilibrium, accordingly. Such behavior is modelled by the previously developed multi-ion charge-regulation model, which considers the effects of the protonation/deprotonation surface reactions, the site density of the functional groups, and pH&salt concentration of the aqueous solution on the silica surface. This boundary condition model forms the basis of the current study.

In the current model, a silica surface with spherical nano patterns with diameter D_R is considered as illustrated in Figure S1. The liquid phase is a KCl (*i.e.* symmetric 1:1) aqueous electrolyte solution consisting of 4 types of ionic species namely; H^+, K^+, Cl^- and OH^- ions with their bulk values being c_{10}, c_{20}, c_{30} and c_{40}, respectively. Due to protonation/deprotonation of ions, the silica surface is charged when in contact with an ionic solution. The surface charge is mainly controlled by the K^+ and Cl^- ions while the pH of the solution is adjusted by the H^+ and OH^- ions. Detailed information on the Poisson-Nernst-Plank (PNP) equations employed in the study is given in the Supporting Information (SI).

Due to the protonation/deprotonation reactions at the solid/liquid interface, the silica channel walls show a charge-regulated behavior depending on the ionic concentration and pH of the ionic aqueous solution. In order to implement this charge regulated nature into the model, two fundamental dissociation/association reactions are considered to be occurring at the solid/liquid interface as follows:

$$SiOH \leftrightarrow SiO^- + H^+ \tag{2}$$

$$SiOH + H^+ \leftrightarrow SiOH_2^+ \tag{3}$$

The equilibrium constants are evaluated by using

View Article Online
DOI: 10.1039/C9CP00706G

$$K_A = \frac{\Gamma_{SiO^-}\left[H^+\right]_w}{\Gamma_{SiOH}},\ K_B = \frac{\Gamma_{SiOH_2^+}}{\Gamma_{SiOH}\left[H^+\right]_w} \tag{4}$$

where Γ_{SiO^-}, Γ_{SiOH} and $\Gamma_{SiOH_2^+}$ are the surface site densities of SiO^-, SiOH and $SiOH_2^+$, respectively and $\left[H^+\right]_w$ is the hydrogen concentration at the solid/liquid interface. In this regard, the surface charge density of the silica walls can be denoted as:

$$\sigma_w = -\frac{F\,\Gamma_{total}}{N_A}\frac{K_A - K_B\left[H^+\right]_w^{\,2}}{K_A + \left[H^+\right]_w + K_B\left[H^+\right]_w^{\,2}} \tag{5}$$

Equation (5) basically determines the difference in number of the charged sites (SiO^- and $SiOH_2^+$), at the final equilibrium of dissociation/association reaction developing on the surface at the corresponding ionic conditions. Similar 2-pK models for dissociation and association reactions have been implemented in the literature for many years due to their success in capturing titration behavior of aqueous silica surface[70]. Later, the direct measurements of such charging sites was accomplished. One of very first proof of surface groups at the silica water interface was done by investigating the oxidation states of surface atoms via XPS measurements[71]. Both O 1s spectra[71] and Si 2p spectra[72] from silica XPS measurements exhibit pH dependent behavior in electron binding energy. Moreover, increasing surface charges by increasing pH described by the charge regulation models was also validated by these experiments.

Results

Our investigations began by calculating ionic distribution over the surfaces with roughness diameter (D_R) of 1nm, 5nm and 10nm. Ionic concentration was varied as C_{KCl}=1mM, 10mM and 100mM while pH was kept constant at 6. Figure 1 presents the electric potential contours of all these cases; each row is the same salt concentration and each column is the same roughness diameter. First, a decrease in salt concentration (i.e; from third row to first row) increases the thickness of EDL such that EDLs growing from facing surfaces of nano-patterns overlap. EDL thickness values smaller than D_R create no overlap that local ionic concentration through the surface remains constant (i.e; D_R=5nm and 20nm at C_{KCl}=1mM or D_R=20nm at C_{KCl}=10mM). However, when the EDL thickness becomes equal or higher than D_R, non-homogenous potential distribution develops on the surface. Here, EDL thickness (λ) normalized with D_R appeared as a

View Article Online
DOI: 10.1039/C9CP00706G

proper representation of the degree of EDL overlap on the surface. Overlapping is initially observed at the bottom of cavities then as λ/D_R increases, overlapping spreads to top of cavities. When the overlapping extends over patterns, bumpy potential distribution on surface becomes rather flat in lateral direction.

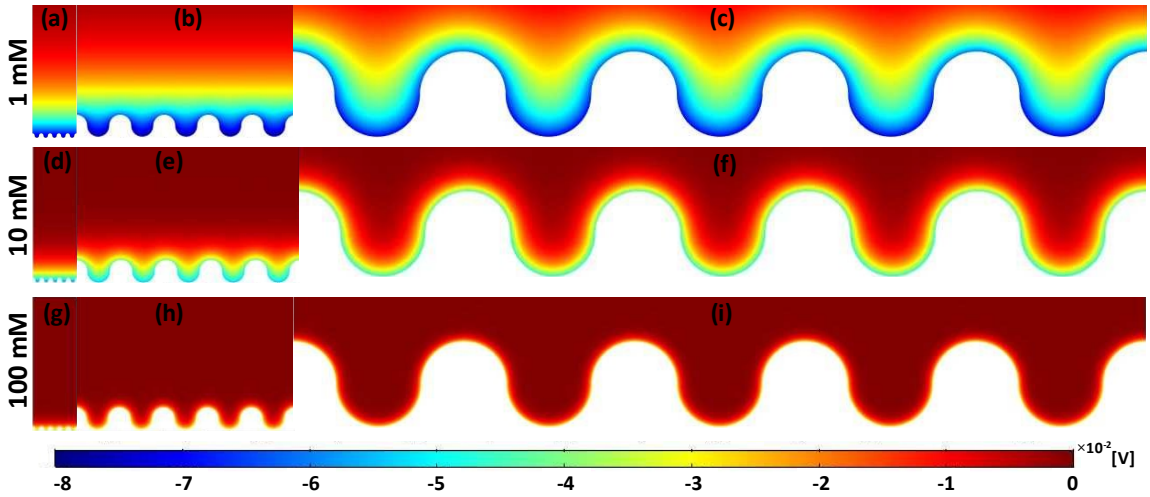

Figure 1. Potential distributions of different concentrations and roughness diameters at pH=6. a-g-d, b-e-h and c-f-i cases have 1 nm, 5 nm and 20 nm diameter roughness values, while a-b-c, d-e-f and g-h-i cases represents 1 mM, 10mM and 100mM salt concentrations, respectively.

Next, we calculated local surface charge densities based on the ionic potential formed on the surface. Figure 2 gives the distribution of surface charge on the surfaces given in Figure 1 along the normalized lateral position (x/D_R). An averaged surface charge density (average of local values) and the PB calculated surface charge density of a flat surface for the same pH and salt concentrations are also given for each case. Different surface charge values develop at different bulk ion concentrations. First, for low λ values with high D_R creating low λ/D_R values, charge is almost constant on the surface and average surface charge is similar to the prediction of flat surface theory. For instance, there is no interaction between EDLs when D_R = 20nm at 10mM and 100mM presented in Figure 1-f and 1-i that surface charge densities given in Figure 2-f and Figure 2-i show only slight variation due to the weak curvature effects on the patterns. However, the increase of λ and/or decrease of D_R yield EDL overlap and stronger curvature effects that surface charge shows

View Article Online
DOI: 10.1039/C9CP00706G

distinct local variations and average surface charge of nano-patterned surface becomes different than the flat surface calculations. Even though as curvature effect increases the absolute value of surface charge as the diameter is decreased[15], EDL overlap decreasing the absolute charge dominates and the average surface charge becomes lower than the absolute charge of a flat surface.

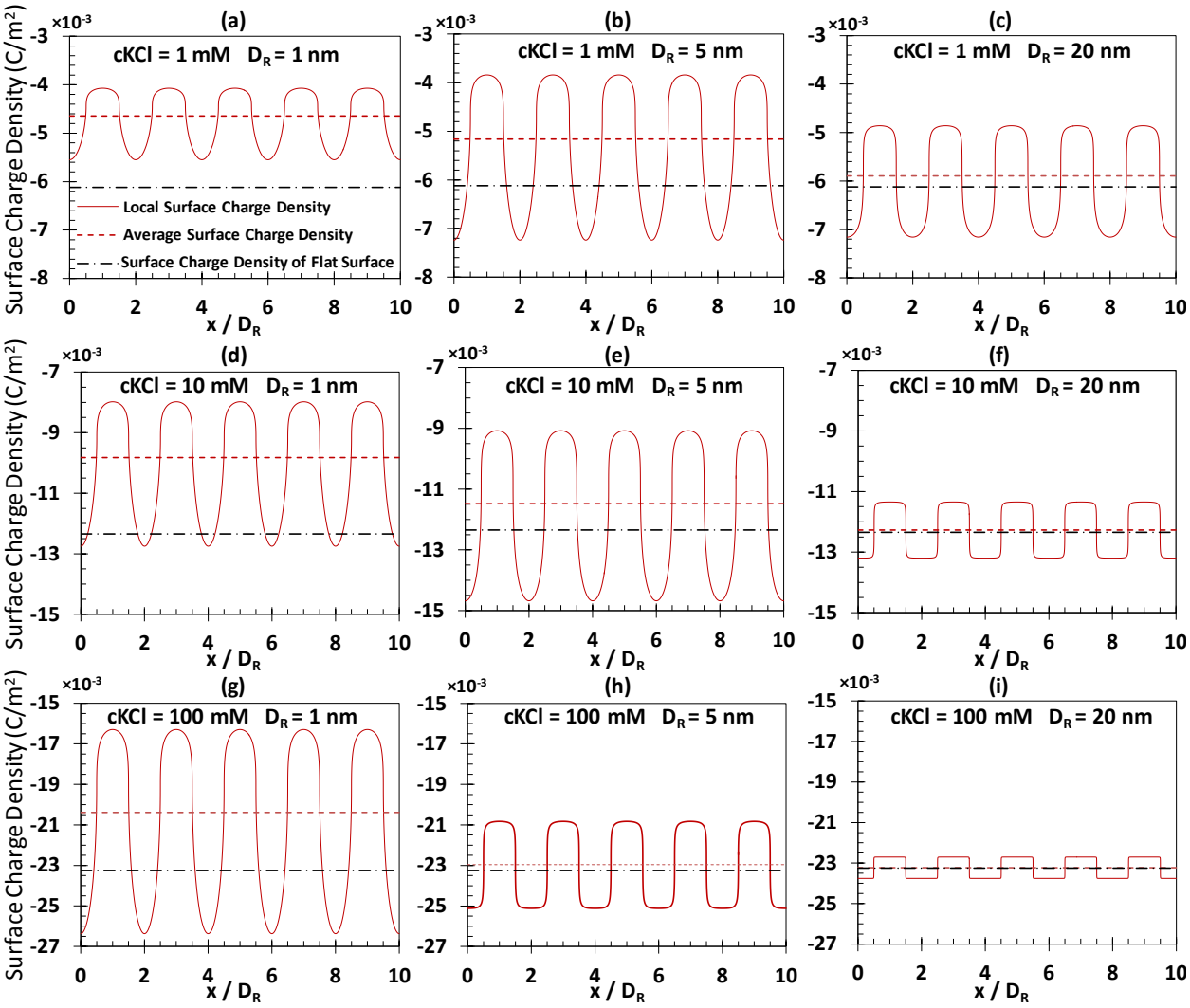

Figure 2. Surface charge density distribution over different rough surfaces at different concentrations (at pH=6). a-g-d, b-e-h and c-f-i cases have 1nm, 5nm and 20nm diameter roughness values, while a-b-c, d-e-f and g-h-I cases represents 1mM, 10mM and 100mM salt concentrations, respectively.

View Article Online
DOI: 10.1039/C9CP00706G

In order to characterize the local charge variation on the nano-patterns, we performed calculations for a wide range of roughness diameters between 1nm to 40nm. Specifically, we measured local surface charge at the tip and the dip of the surface pattern form of half circles. For the comparison, we also calculated surface charge of nanoparticles, as described in another study[15], at the diameter values of the surface roughness. Surface charge results normalized with the theory of flat surface at the corresponding conditions are given in Figure 3 for different salt concentrations of (a) 100mM, (b) 10mM and (c) 1mM. As a first observation, surface charges measured at the tips of rough surface were found identical to the surface charge of a nanoparticle with the same diameter except the overlapped cases. Depending on ionic concentration, EDL overlap develops at different roughness diameters, at which charging behavior on the tip differs from nanoparticle charge behavior. Basically, nanoparticle and tip of surface roughness are almost identical up to diameter of 2nm for the lowest EDL thickness developed at 100mM case, while the divergence at 1mM case starts for diameters smaller than 10nm. Overall, the absolute value of surface charge values at the tip is higher than the flat surface predictions and increases by the decrease of surface roughness. Second, surface charge developing at the dip of valleys showed opposite behavior such that the absolute surface charge was lower than the flat surface and decreased as the roughness diameter decreased. Interestingly, these high and low values cancel each other out so that the average surface charge becomes similar to flat surface charge up to certain roughness dimeters. With the development of EDL overlap governed by both surface roughness and EDL thickness, the absolute value of average surface charge diverges from flat surface calculations.

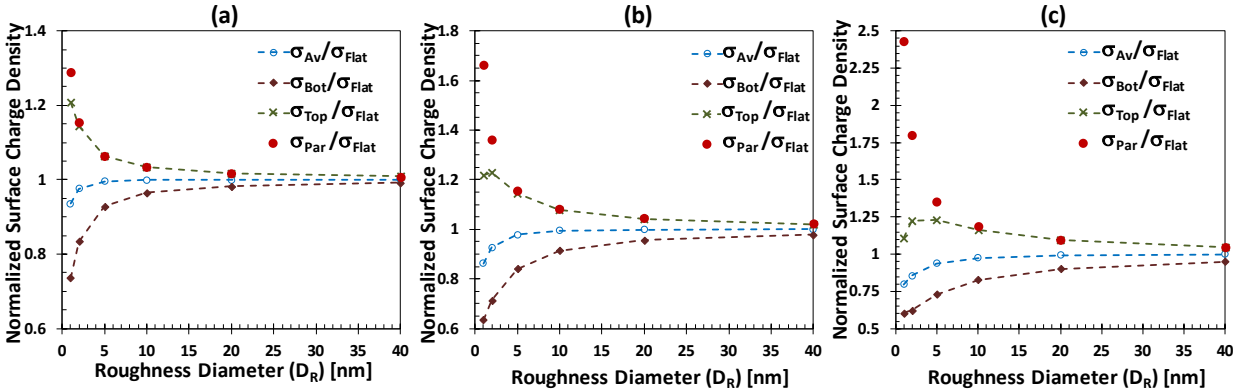

Figure 3. Normalized local charge densities measured on top and bottom of surface pattern for different roughness diameters accompanying with the average surface charge at the (a) 100mM, (b) 10mM and (c) 1mM salt concentrations.

View Article Online
DOI: 10.1039/C9CP00706G

Further characterization based on the overlap ratio (λ/D_R) is performed as a function of pH. In Figure 4(a), the surface charge density on top of the surface pattern normalized with the surface charge of nanoparticle at the same diameter with roughness and pH is presented as a function of pH at different overlap ratios. Curvature effects observed on surface pattern tips creates surface charge values very similar to nanoparticles' surface charge up to $\lambda/D_R = 0.5$ after which overlap growing from the dips alters the surface charge on the tips. As the overlap ratio increases, tips charge becomes lower than nanoparticle counterpart at different levels depending on the pH. Negligible divergence develops at low pH values regardless of overlap ratio, moderate effects are observed for pH values higher than 4, after which an increase of pH enhances the divergence up to pH=6 and then divergence decreases again. Comparison of tip charge with flat surface charge is given in Figure 4(b) for different overlap ratios and pH values. In the absence of EDL overlap at low overlap ratios, surface charge under curvature effects becomes higher that flat surface. Behavior observed for $\lambda/D_R < 0.5$ is similar to results from the literature[15]. The increase of overlap results in decrease of tip charge reaching to flat surface value and going below for low pH values while at high pH value (pH>7) tip charge remained higher than the flat surface.

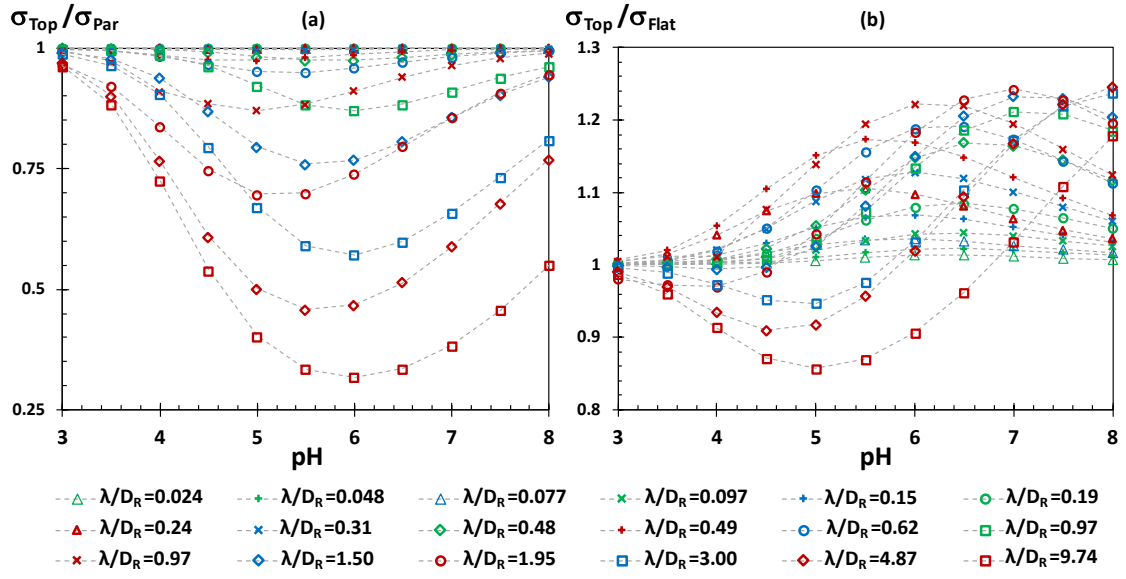

Figure 4. Variation of surface charge density on the top of the surface pattern compared to (a) particle at the dimeter of corresponding roughness and (b) flat surface as a function of pH.

View Article Online
DOI: 10.1039/C9CP00706G

We extended our investigation to joint behavior of tip and dip surface charging, and their average. As the surface reactions governed by the concentration of hydrogen ions (H) on surface, Figure S3 focuses on the surface H concentrations normalized by the flat surface value at the corresponding pH, as a function of overlap ratio and pH. To improve readability, results of pH=3-5.5 and pH=5.5-8 are plotted in two separate graphs. Silica surface develops negative charge between pH=3 to pH=8 silica, the high H concentrations create more protonation resulting in lower absolute surface charges. Two different trends are observed in the general behavior of H concentration at both top and bottom of the pattern. First, H concentration at the bottom decreases with an increase of overlap ratio up to a certain overlap ratio depending on the pH; then trend completely changes that H concentration increases as the overlap increases. An exact opposite behavior is observed on the bottom of pattern. By combining these two behaviors, the average surface charge increases and reaches a constant by the increase of overlap. Overall, the variation of average surface chemistry stops for $\lambda/D_R > 10$ depending on the pH value.

The average surface charges measured on nano-patterned surfaces at different roughness diameters, ionic concentrations, and pH values are summarized in Figure 5. The general behavior shows a decrease in patterned surface charge from flat surface calculations starting from $\lambda/D_R = 0.2$ and higher while nano-roughness mostly becomes effective for $\lambda/D_R>0.5$. Average surface charge becomes independent of surface roughness for high overlaps depending on the pH of the environment. This behavior develops very early at low pH cases ($\lambda/D_R = 2$ for pH<4.5), but moves further to higher $\lambda/D_R > 2$ with the increase of pH. Independent of salt concentration, divergence from theory increases as the pH increases. Charge of patterned surface decreases up to 3/4 of the flat surface value at $\lambda/D_R > 10$ and pH > 6. Overall, the average surface charge density varies between two asymptotes which are at the two limits of surface roughness.

View Article Online
DOI: 10.1039/C9CP00706G

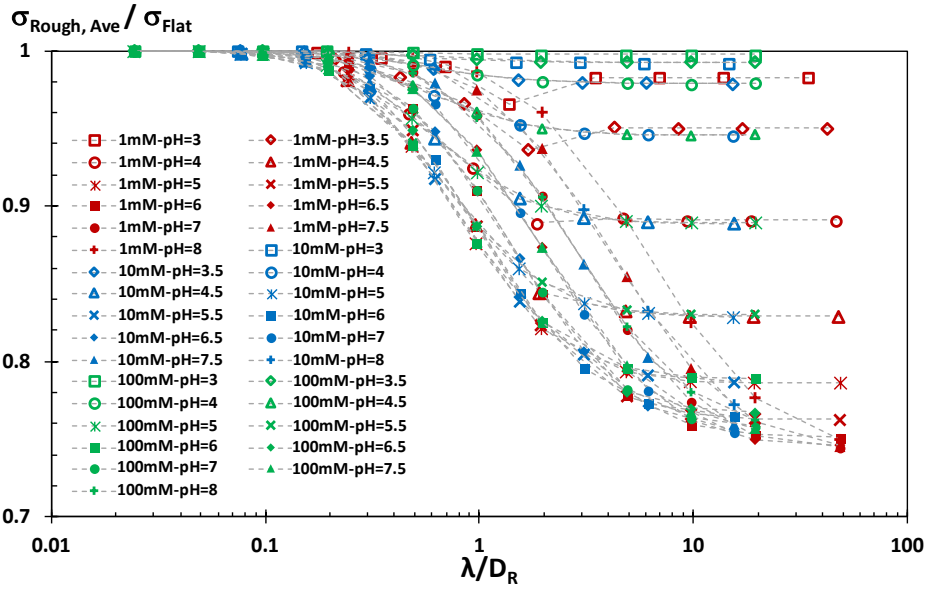

Figure 5. Normalized average surface charge density on the nano-patterned surfaces at different roughness diameters, ionic concentrations, and pH values as a function of overlap ratio.

In Figure 5, average surface charge as a function of overlap ratio shows different behavior depending on ionic concentration and pH. In this extent, it was challenging to normalize this charging behaviors by the ionic properties. However, we also observed that there are certain cases of different salt concentration and pH showing matching variation by the change in overlap. For instance, 1mM at pH=4, 10mM at pH=4.5 and 100mM at pH=5 develops similar average surface charge values as a function of the overlap ratio. To characterize this behavior better, we convert results onto the pH axis in Figure S4. Overall, u-shaped pH dependence shifts from left to right as the overlap increases. For high overlap ratios $\lambda/D_R > 10$, surface charging becomes pH independent for pH values higher than 5.5.

Next, we debated on the effective boundary definition for the electrostatic properties over a rough surface. Effective boundary condition (BC) at a rough surface was investigated for fluid dynamics by many researchers[73–75], but electric BC on a rough surface is mostly overlooked by the literature. As the roughness diameter decreases, surface structures become negligible and surface becomes almost flat. We observed this behavior through the potential distributions given earlier in Figure 1, where electric potential developed over small surface roughness (Figure 1(a), (d) and (g)) shows a smooth distribution. Electric properties over a surface is not the result of surface roughness only, instead it is formed by the ratio of EDL thickness to surface roughness.

View Article Online
DOI: 10.1039/C9CP00706G

Hence, electric potentials are flattened even at moderate surface roughness at high overlap ratios as can be seen from Figure 1(b). Furthermore, any electrostatic or electrokinetic interaction between an object and a rough/patterned surface would be governed by the electric properties at the effective boundary region rather than the electric charge at the bottom of surface patterns. Based on this perspective, we studied the average electric potential measured through a line passing through the tips of pattern parallel to the surface. The average electric potential measured on tip line BC at different roughness diameters, ionic concentrations, and pH values are given in Figure 6. These are the same cases at which surface charge values calculated in the earlier Figure 5 through surface arc length path. The average electric potential on top BC of the nanopatterns normalized with flat surface potential increases by the increase of overlap ratio; starting from a zero potential at $\lambda/D_R \rightarrow 0$, tip line BC reaches to flat surface theory and remains constant for $\lambda/D_R > 10$. This is a very interesting and expected behavior. Very low λ/D_R makes tip line BC remain in the bulk of EDL where negative and positive ions are at equal number, creating a zero-net electric potential. On the other end, high λ/D_R results in flattened surface and surface potential that roughness effects disappear, and surface charging behaves almost like a flat surface, except the pH dependence. Let's remember that normalization is done by the flat surface value at the corresponding pH. At low λ/D_R values ($\lambda/D_R < 0.5$), pH dependence of tip line BC is very similar to flat surfaces in that all results remain on the same line. However, with the increase of λ/D_R, potential values show a variation the change of pH. Results at different ionic concentrations continue to show very similar behavior, which shows that ionic concentration effects were successfully normalized by the λ/D_R definition. At high λ/D_R values, high pH values gave identical results with flat surface, but low pH created higher potential values than the flat surface calculations.

We further studied the pH dependence of boundary potential in Figure S5 presenting normalized boundary potential as a function pH. There was no significant pH dependence on boundary potential observed up to $\lambda/D_R = 1$ that potential remains as a constant flat line in Figure S5. For higher overlap ratio ($\lambda/D_R > 1$), normalized boundary potential increases by the decrease in pH.

View Article Online
DOI: 10.1039/C9CP00706G

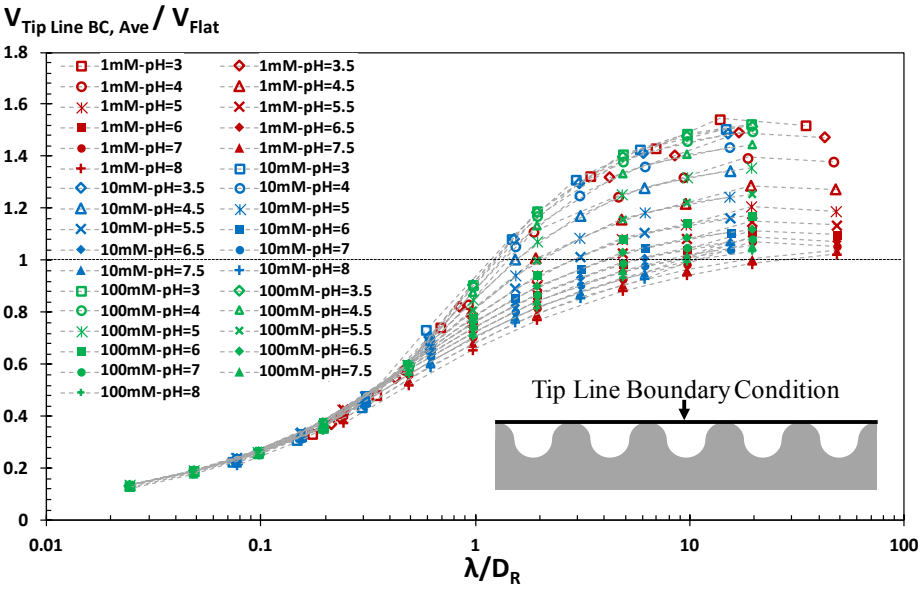

Figure 6. Normalized average surface potential on the nano-patterned surfaces at different roughness diameters, ionic concentrations, and pH values as a function of overlap ratio.

In an attempt to provide an easy to use phenomenological model, we developed an empirical model as a fit on our numerical results. In this context, we found Equation (6) from the trigonometric functions family to be the best fit for the observed variation of surface charge by the variation of the overlap ratio. As the $\lambda/D_R \rightarrow 0$, Equation (6) gets the value of unity representing the cases of negligible overlap where surface charge on a rough surface is equal to the theoretical predictions. At the other end where $\lambda/D_R \rightarrow \infty$, Equation (6) approaches to $1-a$, as the parameter a accounts for the variation from the theory. Therefore, Equation (6) can simply model the variation of normalized charge of rough surfaces between the two asymptotes of 1 and $1-a$ while the surface charge values in between develops as a function of overlap ratio and parameter b.

$$\frac{\sigma_{Rough,Ave}}{\sigma_{Flat}} = 1 - a\frac{b(\lambda/D_R)^2}{b(\lambda/D_R)^2+1} \qquad (6)$$

The two parameters of Equation (6), a and b, depend on pH and salt concentration of the ionic solution. Next, we studied the variation of these parameters by fitting the Equation (6) on all of the calculations in Figure S6. The a and b parameters showed variation between two asymptotes with opposite behavior that hyperbolic trigonometric functions given in Equation (7) and (8) are able to provide a universal description for all of the studied cases.

View Article Online
DOI: 10.1039/C9CP00706G

$$a = \frac{pK_A - pK_B}{40}\left[1 + Tanh\left(pH - pK_A + pK_B - \frac{\log[KCl] - 1}{2}\right)\right] \quad (7)$$

$$b = \frac{pK_A - pK_B}{4}\left[1 - Tanh\left(pH - pK_A + pK_B - \frac{\log[KCl] - 4}{2}\right)\right] \quad (8)$$

Predictions of Equation (6) using Equation (7) and (8) showed very good agreement with the numerical results. In Figure 7, relative errors between our empirical model and numerical results are shown for all cases as a function of overlap ratio. Overall, there is no more than 4% difference between empirical model and the numerical calculations. For the overlap ratios less than 0.1 where surface roughness effects are negligible, our model can capture flat surface theory very precisely with a relative error of less than 0.2%. With the increase of overlap ratio, relative error shows variation case by case, but average relative error of our model remains less than 1%. Hence, the proposed model successfully predicts the deviation of surface charge density due to roughness effects as an extension to flat surface theory. It is important to mention that flat surface theory and so this new extension model is applicable on cases where continuum assumption remained valid. This means D_R values less than certain scales (D_R<~1nm) cannot be predicted by PNP or by our model (Equation (6)). We should also note that this model calculates the average surface charge through the arc length path of surface roughness; however, Figure 7 suggests that as the overlap ratio approaches to 10 ($\lambda/D_R \rightarrow 10$), electric potential on rough surface flattens and the surface charge effective on physical mechanism approaches back to flat surface value.

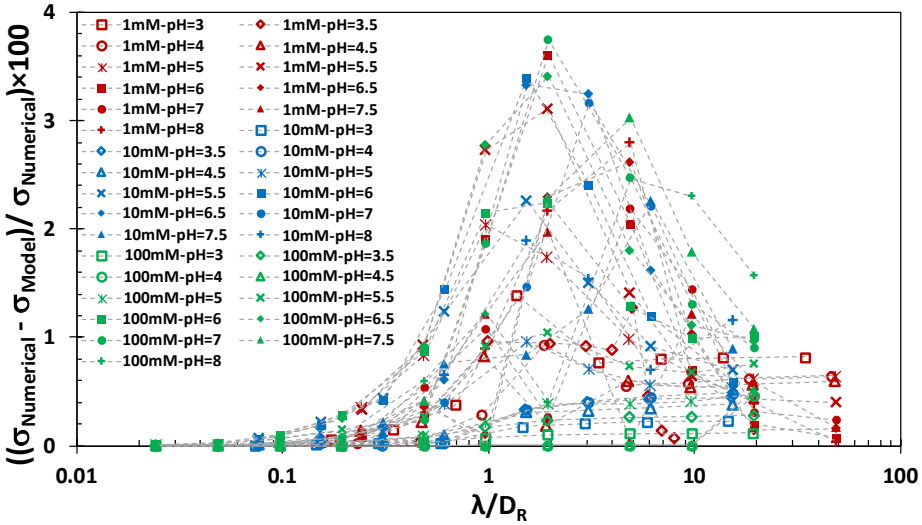

View Article Online
DOI: 10.1039/C9CP00706G

Figure 7. Percentile of the relative error between the surface charge predictions of the empirical model (Equation (6), (7) and (8)) and numerical results at different roughness diameters, ionic concentrations, and pH.

Discussion

A representative nano-patterned surface in the form of repeating concave and convex circles is studied due to two advantages. First, we can control surface structures by varying the single quantity, D_R, and perform a parametric study by systematically varying it. Second, since the tip of the circles developed curvature effect similar to nanoparticles, we can validate our calculations with our earlier work on nanoparticles [19] which was validated by experiments. Until the overlap effects growing from the pits dominate, nanopattern tip surface charges by decreasing size are identical to the surface charge of the nanoparticle at the corresponding size.

Overall, surface electric charging on a nano-patterned surface is equal to charge of a flat surface until the size of the structure becomes comparable with the corresponding EDL thickness. We characterized such formations using the non-dimensional Debye length definition which was employed to investigate non-uniform behavior of surface electrostatics by many researchers in various forms; such as normalized by the particle diameter (λ/D_p)[15], distance between particle and surface (λ/h)[58], channel lenght (λ/L)[76] and channel height (λ/H)[76]. For our case, ratio of EDL thickness to roughness diameter as λ/D_R could represent both curvature effects on the tips and overlap effects in the pits of roughness. Both of these effects creating divergence from regular flat surface theory develop with the decrease of nano-pattern size represented by roughness diameter or by the increase of EDL thickness. For such cases, comparable variation of D_R and λ defines the surface charging that a very small D_R with a very small λ and a moderately small D_R with a moderately small λ creates similar behaviors. The λ/D_R offers insight about the general trend which can be divided into three behaviors; with the increase of λ/D_R, (i) slight divergence from the flat surface charge value, (ii) significant increase up to a maximum deviation, and (iii) reaming constant at this maximum value. The general mechanisms can be explained as follows; initially, for a high salt concentration and for a high roughness diameter ($\lambda/D_R \rightarrow 0$), diffuse layer can form completely parallel to surface morphology that rough surface develops flat surface's electrostatics. As thickness of diffuse layer increases (or roughness diameter decreases), first, overlap occurs at the bottom of surface structures increasing potential and causing more protonation and decreasing

View Article Online
DOI: 10.1039/C9CP00706G

absolute surface charge. Second, curvature effects develop at the tip of structures decreasing potential and protonation that increases the absolute surface charge. Interestingly, for low λ/D_R values, these two cancel each other out until the overlap growing by the increasing λ/D_R dominates and decreases the average surface charge values on nano-patterned surface.

Further characterizations are required to determine the physically effective charge on the patterned surface for high λ/D_R cases. The high λ/D_R at either small surface patterns or big EDL thicknesses repress local variation on the patterned surface such that potential distribution becomes almost flat. This simply suggests that surface heterogeneity effects on electrokinetics almost disappears for high λ/D_R. Especially for low pattern sizes, interaction on the nano-patterned surface should not be expected to develop through the electrostatic properties deep inside the pits of the patterns, instead effective electrokinetics will be governed by the properties through a region on top of surface patterns. For such a case, tip line boundary condition is an idea to approach this behavior. Since we are not on a surface, we measured electric potential instead of a charge value on the effective line BC. Variation of electric potential on the line BC by the variation of λ/D_R is different than the behavior of the surface charge measured through the arch length of surface patterns. Simply, at low λ/D_R values, ionic accumulation (EDL) is mostly confined inside the nano-patterns such that average potential on tip line BC is almost zero; for these cases current line BC may not be appropriate. For instance, for large D_R cases, electrokinetic interactions are expected to develop through arc length of surface patterns, not through the tip line BC. By increasing λ/D_R, ionic layering grows out of surface patterns such that average potential at the tip line increases. First, it reaches flat surface potential and then to a constant value of equal or higher than flat surface's potential depending on the pH value. For example, at pH=8, tip line potential measured at different salt concentrations reaches to flat surface potential and remains constant by the increase of λ/D_R. However, lower pH values exceed flat surface potential. This specific behavior is mostly attributed to a difference between the pH dependence of potential on a surface and potential on a line BC. In general, comparisons (or normalizations) are done by the flat surface value at the corresponding pH value. With the decrease of pH, flat surface potential decreases while the tip line potential decreases slower; hence, at low pH values tip line potential becomes higher than flat surface potential.

View Article Online
DOI: 10.1039/C9CP00706G

As a final remark, current calculations are based on the continuum approximations which is not valid at the certain nanoscale limits. The primary surface charging develops on the binding sites which is usually described by the site density per area. While the different experimental procedures reported different results, site density for silica is mostly measured between 5 to 11 sites/nm^2.[88] There are positively and negatively charged surface groups distributed on these binding sites and the continuum description of corresponding surface charge is approximated by the average of these surface groups. Such an average definition will not be appropriate for small bodies since there will not be enough binding sites for a proper statistical averaging. Hence, current continuum calculations and proposed empirical model are not appropriate to estimate surface charging of nonpattern sizes smaller than ~2-3nm. These size values mostly yield $\lambda/D_R > 10$ case, which were carried on for the purpose of observing the extent of charging behavior in its limits to properly define the proposed empirical model in the corresponding mathematical limits.

Current results proved that surface heterogeneity creates dominant effects on surface charge formations. While such behavior creates complications for many applications (such as AFM), it can also be advantageous for future technologies. Nano-engineered surfaces can be designed with a desired surface charging for a specific task. Our results for a sample circular surface pattern can be directly used for surface patterning using nanoparticles. On the other end, AFM measurements should incorporate surface charge influence of surface heterogeneity. Considering physical heterogeneity aspect of roughness only results in wrong estimation for surface forces measured in an ionic solution.

Conclusion

This study characterized the charge density of patterned silica surfaces. In contrast to many studies which consider surface charge independent of the surface topography, this study calculated the effects of surface structures onto surface charging. Using the numerical solution of ionic equilibrium based on PNP equation with Charge Regulation boundaries, we found that surface charge density is not just a material property but is dependent on the size of surface roughness in addition to the solution conditions. In this regard, we calculated the local surface charge density based on the local ionic concentrations for different scenarios such as various surface pattern sizes and solution parameters. Through such a systematic approach, we evaluated both local and average surface charge density of the patterned surfaces and associated the EDL overlap and curvature

View Article Online
DOI: 10.1039/C9CP00706G

effects developing on the surface pattern. In general, as surface structure diameter decreased, EDL overlap developed in the pits of surface pattern decreasing the surface charge value of effected regions, while curvature effect developed at the tips of the pattern increasing the corresponding local surface charges. Hence, the homogeneous surface charge assumption is very much invalid since charge values at the pits can be half and at the tips can be double of the predictions for a flat surface. Furthermore, we characterized simultaneous behavior of these two mechanisms creating opposite effects by defining and calculating an average charge value through the symmetrical surface pattern. For our simple representative pattern made of repeating circular dips and tips of identical size, decreases in surface charge at the dips and increases in the tips cancels each other up to a certain value of surface pattern size and ionic concentration that average surface charge remains the same as the surface charge of a flat surface. Further characterization was performed by combining the effect of pattern size and ionic condition as overlap ratio (λ/D_R). As the overlap ratio reached and exceeded the value of 0.2, average surface charge of a patterned surface became less than flat surface predictions and decreased further up to a certain asymptotic value depending strongly on pH. By increasing the overlap ratio, electric potential distribution over patterned surface becomes less bumpy and/or becomes flatter which is the physical mechanism behind the convergence of average surface charge to an asymptote at high overlap ratio limit. For such a case, a flatter boundary definition will be required to define the average surface charge effective on the surface, instead of surface charge on the arc length path of surface pattern. Based on this idea, we further measured average electric potential on a line boundary condition passing through the tips of surface pattern which was found to be converging to flat surface charge at the high overlap ratio limit. Using the numerical results, a phenomenological model describing the deviation of average charge density of a patterned/rough from the flat surface theory is developed. The proposed model extends the existing theory as a function of surface pattern size, ionic concentration, pH and constants of surface charge group chemistry, successfully.

View Article Online
DOI: 10.1039/C9CP00706G

TOC Graphic

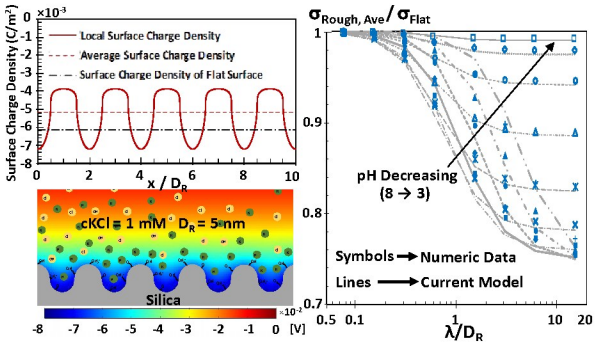

View Article Online
DOI: 10.1039/C9CP00706G

Supporting Information Additional details of chemical models and calculations.

Acknowledgements This work was supported by the Scientific and Technological Research Council of Turkey (TÜBİTAK) under the Grant Number 118M710 and Izmir Institute of Technology Research Funds under the Grant Number 2017-IYTE-57. Authors also would like to thank Center for Scientific Computation at Southern Methodist University.

References

1 M. Fuest, K. K. Rangharajan, C. Boone, A. T. Conlisk and S. Prakash, Cation Dependent Surface Charge Regulation in Gated Nanofluidic Devices, *Anal. Chem.*, 2017, **89**, 1593–1601.

2 A. T. Celebi, M. Barisik and A. Beskok, Surface charge-dependent transport of water in graphene nano-channels, *Microfluid. Nanofluidics*, , DOI:10.1007/s10404-017-2027-z.

3 X. Gao, A. Omosebi, N. Holubowitch, J. Landon and K. Liu, Capacitive Deionization Using Alternating Polarization: Effect of Surface Charge on Salt Removal, *Electrochim. Acta*, 2017, **233**, 249–255.

4 I. Larson, C. J. Drummond, D. Y. C. Chan and F. Grieser, Direct force measurements between titanium dioxide surfaces, *J. Am. Chem. Soc.*, 1993, **115**, 11885–11890.

5 A. Klaassen, F. Liu, D. van den Ende, F. Mugele and I. Siretanu, Impact of surface defects on the surface charge of gibbsite nanoparticles, *Nanoscale*, 2017, **9**, 4721–4729.

6 C. von Roemeling, W. Jiang, C. K. Chan, I. L. Weissman and B. Y. S. Kim, *Trends Biotechnol.*, 2017, 35, 159–171.

7 B. J. Feinberg, J. C. Hsiao, J. Park, A. L. Zydney, W. H. Fissell and S. Roy, Silicon nanoporous membranes as a rigorous platform for validation of biomolecular transport models, *J. Memb. Sci.*, 2017, **536**, 44–51.

8 Y. Zhang, G. Wu, W. Si, J. Ma, Z. Yuan, X. Xie, L. Liu, J. Sha, D. LI and Y. Chen, Ionic current modulation from DNA translocation through nanopores under high ionic strength and concentration gradients, *Nanoscale*, 2016, 930–939.

9 G. Huang, K. Willems, M. Soskine, C. Wloka and G. Maglia, Electro-osmotic capture and ionic discrimination of peptide and protein biomarkers with FraC nanopores, *Nat. Commun.*, , DOI:10.1038/s41467-017-01006-4.

View Article Online
DOI: 10.1039/C9CP00706G

10 E. Priyadarshini and N. Pradhan, *Sensors Actuators, B Chem.*, 2017, 238, 888–902.

11 S. Brosel-Oliu, D. Galyamin, N. Abramova, F. X. Muñoz-Pascual and A. Bratov, Impedimetric label-free sensor for specific bacteria endotoxin detection by surface charge registration, *Electrochim. Acta*, 2017, **243**, 142–151.

12 R. F. Probstein, *Physicochemical hydrodynamics: an introduction*, John Wiley & Sons, 2005.

13 J. H. Masliyah and S. Bhattacharjee, *Electrokinetic and colloid transport phenomena*, John Wiley & Sons, 2006.

14 M. Kobayashi, F. Juillerat, P. Galletto, P. Bowen and M. Borkovec, Aggregation and charging of colloidal silica particles: Effect of particle size, *Langmuir*, 2005, **21**, 5761–5769.

15 M. Barisik, S. Atalay, A. Beskok and S. Z. Qian, Size Dependent Surface Charge Properties of Silica Nanoparticles, *J. Phys. Chem. C*, 2014, **118**, 1836–1842.

16 F. Borghi, V. Vyas, A. Podestà and P. Milani, Nanoscale Roughness and Morphology Affect the IsoElectric Point of Titania Surfaces, *PLoS One*, , DOI:10.1371/journal.pone.0068655.

17 J. F. L. Duval, F. A. M. Leermakers and H. P. Van Leeuwen, Electrostatic interactions between double layers: Influence of surface roughness, regulation, and chemical heterogeneities, *Langmuir*, 2004, **20**, 5052–5065.

18 X. Yang and G. Zhang, The effect of an electrical double layer on the voltammetric performance of nanoscale interdigitated electrodes: A simulation study, *Nanotechnology*, , DOI:10.1088/0957-4484/19/46/465504.

19 L. C. Hsu, J. Fang, D. A. Borca-Tasciuc, R. W. Worobo and C. I. Moraru, Effect of micro- and nanoscale topography on the adhesion of bacterial cells to solid surfaces, *Appl. Environ. Microbiol.*, 2013, **79**, 2703–2712.

20 O. Rzhepishevska, S. Hakobyan, R. Ruhal, J. Gautrot, D. Barbero and M. Ramstedt, The surface charge of anti-bacterial coatings alters motility and biofilm architecture, *Biomater. Sci.*, 2013, **1**, 589.

21 A. L. Božič, From discrete to continuous description of spherical surface charge distributions, *Soft Matter*.

22 M. A. Blanco and V. K. Shen, Effect of the surface charge distribution on the fluid phase

View Article Online
DOI: 10.1039/C9CP00706G

behavior of charged colloids and proteins, *J. Chem. Phys.*, 2016, **145**, 155102.

23 A. I. Abrikosov, B. Stenqvist and M. Lund, Steering patchy particles using multivalent electrolytes, *Soft Matter*, 2017, **13**, 4591–4597.

24 E. Bianchi, P. D. J. van Oostrum, C. N. Likos and G. Kahl, *Curr. Opin. Colloid Interface Sci.*, 2017, 30, 8–15.

25 A. D. Stroock and G. M. Whitesides, *Acc. Chem. Res.*, 2003, 36, 597–604.

26 K. Ward and Z. H. Fan, Mixing in microfluidic devices and enhancement methods, *J. Micromechanics Microengineering*, , DOI:10.1088/0960-1317/25/9/094001.

27 Y. Yang, K. Webb, Y. Liu, K. Liu and Z. Nie, *Synthesis, Self-Assembly, and Applications of Amphiphilic Janus and Triblock Janus Nanoparticle Analogs*, World Scientific, 2017.

28 van N. Danny, in *Bioreactors*, 2016.

29 M. Karle, S. K. Vashist, R. Zengerle and F. von Stetten, *Anal. Chim. Acta*, 2016, 929, 1–22.

30 S. G. Elci, Y. Jiang, B. Yan, S. T. Kim, K. Saha, D. F. Moyano, G. Yesilbag Tonga, L. C. Jackson, V. M. Rotello and R. W. Vachet, Surface Charge Controls the Suborgan Biodistributions of Gold Nanoparticles, *ACS Nano*, 2016, **10**, 5536–5542.

31 E. Palleau, L. Ressier, Borowik and T. Mélin, Numerical simulations for a quantitative analysis of AFM electrostatic nanopatterning on PMMA by Kelvin force microscopy, *Nanotechnology*, , DOI:10.1088/0957-4484/21/22/225706.

32 J. P. Hoogenboom, D. L. J. Vossen, C. Faivre-Moskalenko, M. Dogterom and A. van Blaaderen, Patterning surfaces with colloidal particles using optical tweezers, *Appl. Phys. Lett.*, 2002, **80**, 4828–4830.

33 R. Parthasarathy, P. A. Cripe and J. T. Groves, Electrostatically driven spatial patterns in lipid membrane composition, *Phys. Rev. Lett.*, , DOI:10.1103/PhysRevLett.95.048101.

34 M. Sayin and R. Dahint, Formation of charge-nanopatterned templates with flexible geometry via layer by layer deposition of polyelectrolytes for directed self-assembly of gold nanoparticles, *Nanotechnology*, 2017, **28**, 135303.

35 R. M. Fillion, A. R. Riahi and A. Edrisy, A review of icing prevention in photovoltaic devices by surface engineering, *Renew. Sustain. Energy Rev.*, 2014, **32**, 797–809.

36 L. Zhang, N. Zhao and J. Xu, Fabrication and application of superhydrophilic surfaces: A review, *J. Adhes. Sci. Technol.*, 2014, **28**, 769–790.

View Article Online
DOI: 10.1039/C9CP00706G

37 A. Koklu, A. Mansoorifar and A. Beskok, Self-Similar Interfacial Impedance of Electrodes in High Conductivity Media, *Anal. Chem.*, 2017, **89**, 12533–12540.

38 P. Zhang and S. Wang, *ChemPhysChem*, 2014, 15, 1550–1561.

39 B. Derjaguin and L. Landau, The theory of stability of highly charged lyophobic sols and coalescence of highly charged particles in electrolyte solutions, *Acta Physicochim. URSS*, 1941, **14**, 58.

40 E. J. W. Verwey, Theory of the stability of lyophobic colloids., *J. Phys. Chem.*, 1947, **51**, 631–636.

41 J. T. G. Overbeek and E. J. W. Verwey, *Theory of the Stability of Lyophobic Colloids: The interaction of Sol Particles Having an Electric Double Layer*, Elsevier, New York, 1948.

42 E. M. V Hoek, S. Bhattacharjee and M. Elimelech, Effect of membrane surface roughness on colloid-membrane DLVO interactions, *Langmuir*, 2003, **19**, 4836–4847.

43 X. Huang, S. Bhattacharjee and E. M. V Hoek, Is surface roughness a 'scapegoat' or a primary factor when defining particle-substrate interactions?, *Langmuir*, 2010, **26**, 2528–2537.

44 M. Bendersky and J. M. Davis, DLVO interaction of colloidal particles with topographically and chemically heterogeneous surfaces, *J. Colloid Interface Sci.*, 2011, **353**, 87–97.

45 N. Kumar, C. Zhao, A. Klaassen, D. Van den Ende, F. Mugele and I. Siretanu, Characterization of the surface charge distribution on kaolinite particles using high resolution atomic force microscopy, *Geochim. Cosmochim. Acta*, 2016, **175**, 100–112.

46 C. Zhao, D. Ebeling, I. Siretanu, D. van den Ende and F. Mugele, Extracting local surface charges and charge regulation behavior from atomic force microscopy measurements at heterogeneous solid-electrolyte interfaces, *Nanoscale*, 2015, **7**, 16298–16311.

47 G. Trefalt, S. H. Behrens and M. Borkovec, Charge Regulation in the Electrical Double Layer: Ion Adsorption and Surface Interactions, *Langmuir*, 2016, **32**, 380–400.

48 B. W. Ninham and V. A. Parsegian, Electrostatic potential between surfaces bearing ionizable groups in ionic equilibrium with physiologic saline solution, *J. Theor. Biol.*, 1971, **31**, 405–428.

49 V. E. Shubin and P. Kékicheff, Electrical Double Layer Structure Revisited via a Surface Force Apparatus: Mica Interfaces in Lithium Nitrate Solutions, *J. Colloid Interface Sci.*,

View Article Online
DOI: 10.1039/C9CP00706G

1993, **155**, 108–123.

50 J. P. Chapel, Electrolyte Species Dependent Hydration Forces between Silica Surfaces, *Langmuir*, 1994, **10**, 4237–4243.

51 M. Dishon, O. Zohar and U. Sivan, From repulsion to attraction and back to repulsion: The effect of NaCl, KCl, and CsCl on the force between silica surfaces in aqueous solution, *Langmuir*, 2009, **25**, 2831–2836.

52 I. Popa, P. Sinha, M. Finessi, P. Maroni, G. Papastavrou and M. Borkovec, Importance of charge regulation in attractive double-layer forces between dissimilar surfaces, *Phys. Rev. Lett.*, , DOI:10.1103/PhysRevLett.104.228301.

53 K. Da Huang and R. J. Yang, Electrokinetic behaviour of overlapped electric double layers in nanofluidic channels, *Nanotechnology*, , DOI:10.1088/0957-4484/18/11/115701.

54 A. Golovnev and S. Trimper, Steady state solution of the Poisson-Nernst-Planck equations, *Phys. Lett. Sect. A Gen. At. Solid State Phys.*, 2010, **374**, 2886–2889.

55 R. Nosrati, M. Hadigol, M. Raisee and A. Nourbakhsh, Numerical modeling of electroosmotic nanoflows with overlapped electric double layer, *J. Comput. Theor. Nanosci.*, 2012, **9**, 2228–2239.

56 J. K. Holt, H. G. Park, Y. Wang, M. Stadermann, A. B. Artyukhin, C. P. Grigoropoulos, A. Noy and O. Bakajin, Fast mass transport through sub-2-nanometer carbon nanotubes, *Science (80-.).*, 2006, **312**, 1034–1037.

57 H. Verweij, M. C. Schillo and J. Li, Fast mass transport through carbon nanotube membranes, *Small*, 2007, **3**, 1996–2004.

58 S. Atalay, M. Barisik, A. Beskok and S. Qian, Surface charge of a nanoparticle interacting with a flat substrate, *J. Phys. Chem. C*, 2014, **118**, 10927–10935.

59 G. Karniadakis, A. Beskok and N. Aluru, 2005.

60 D. Li, *Electrokinetics In Microfluidics*, Elsevier/Academic Press, 2004.

61 S. Qian and Y. Ai, *Electrokinetic Particle Transport In Micro-/Nanofluidics*, CRC Press, Boca Raton, 2012.

62 M. Polat and H. Polat, Analytical solution of Poisson-Boltzmann equation for interacting plates of arbitrary potentials and same sign, *J. Colloid Interface Sci.*, 2010, **341**, 178–185.

63 Y. Ma, Y. S. Su, S. Qian and L. H. Yeh, Analytical model for surface-charge-governed nanochannel conductance, *Sensors Actuators, B Chem.*, 2017, **247**, 697–705.

View Article Online
DOI: 10.1039/C9CP00706G

64 W. Qu and D. Li, A model for overlapped EDL fields, *J. Colloid Interface Sci.*, 2000, **224**, 397–407.

65 C. L. Ren, Y. Hu, D. Li and C. Werner, A new model for the electrical double layer interaction between two surfaces in aqueous solutions, *J. Adhes.*, , DOI:10.1080/00218460490480824.

66 B. J. Kirby, *Micro-Nanoscale Fluid Mechanics Transport in Microfluidic Devices*, Cornell University, New York, 2010.

67 Y.-J. Oh, A. L. Garcia, D. N. Petsev, G. P. Lopez, S. R. J. Brueck, C. F. Ivory and S. M. Han, Effect of wall–molecule interactions on electrokinetic transport of charged molecules in nanofluidic channels during FET flow control, *Lab Chip*, 2009, **9**, 1601.

68 M. Zhang, L. H. Yeh, S. Qian, J. P. Hsu and S. W. Joo, DNA electrokinetic translocation through a nanopore: Local permittivity environment effect, *J. Phys. Chem. C*, 2012, **116**, 4793–4801.

69 D. Jing and B. Bhushan, Electroviscous effect on fluid drag in a microchannel with large zeta potential, *Beilstein J. Nanotechnol.*, 2015, **6**, 2207–2216.

70 M. A. Brown, M. Arrigoni, F. Héroguel, A. Beloqui Redondo, L. Giordano, J. A. Van Bokhoven and G. Pacchioni, PH dependent electronic and geometric structures at the water-silica nanoparticle interface, *J. Phys. Chem. C*, 2014, **118**, 29007–29016.

71 Y. Duval, J. A. Mielczarski, O. S. Pokrovsky, E. Mielczarski and J. J. Ehrhardt, Evidence of the existence of three types of species at the quartz-aqueous solution interface at pH 0-10: XPS surface group quantification and surface complexation modeling, *J. Phys. Chem. B*, 2002, **106**, 2937–2945.

72 M. A. Brown, A. Beloqui Redondo, M. Sterrer, B. Winter, G. Pacchioni, Z. Abbas and J. A. Van Bokhoven, Measure of surface potential at the aqueous-oxide nanoparticle interface by XPS from a liquid microjet, *Nano Lett.*, 2013, **13**, 5403–5407.

73 Y. Achdou, O. Pironneau and F. Valentin, Effective Boundary Conditions for Laminar Flows over Periodic Rough Boundaries, *J. Comput. Phys.*, 1998, **147**, 187–218.

74 S. Veran, Y. Aspa and M. Quintard, Effective boundary conditions for rough reactive walls in laminar boundary layers, *Int. J. Heat Mass Transf.*, 2009, **52**, 3712–3725.

75 J. Guo, S. Veran-Tissoires and M. Quintard, Effective surface and boundary conditions for heterogeneous surfaces with mixed boundary conditions, *J. Comput. Phys.*, 2016, **305**,

View Article Online
DOI: 10.1039/C9CP00706G

942–963.

76 T. Sen and M. Barisik, Size dependent surface charge properties of silica nano-channels: double layer overlap and inlet/outlet effects, *Phys. Chem. Chem. Phys.*, 2018, **20**, 16719–16728.